Differential Pulse-Position Modulation for Power-Efficient Optical Communication

Da-shan Shiu, *Student Member, IEEE,* and Joseph M. Kahn, *Senior Member, IEEE*

***Abstract*— In this paper, we examine the use of differential pulse-position modulation (DPPM) for optical communication systems using intensity modulation with direct detection in the presence of additive white Gaussian noise. We present expressions for the error probability and power spectral density of DPPM. We show that for a given bandwidth, DPPM requires significantly less average power than pulse-position modulation (PPM). We also examine the performance of DPPM in the presence of multipath intersymbol interference (ISI). We find that the ISI penalties incurred by PPM and DPPM exhibit very similar dependencies upon the channel rms delay spread. We discuss the use of chip-rate and multichip-rate equalization to combat ISI. Finally, we describe potential problems caused by the nonuniform bit-rate characteristic of DPPM, and we propose several solutions.**

***Index Terms*—Differential pulse-position modulation, intensity modulation, wireless optical communication.**

I. Introduction

WIRELESS indoor communication is drawing increasing attention as an emerging technology [1]. Transmission using infrared radiation has recently become a viable option. As a transmission medium, infrared offers several advantages over radio, including a virtually unlimited spectral region that is not regulated worldwide, relative security against eavesdropping, reuse of the same spectrum in every room of a building without interference, and immunity to multipath fading. Many applications of infrared links require high average-power efficiency to minimize ocular hazards [2] and power consumption. Pulse-position modulation (PPM) is a technique that achieves very good average-power efficiency and is widely used in these applications. For example, the infrared data association (IrDA) has designated 4-PPM as the standard modulation technique for 4-Mb/s serial data links [3], [4]. The National Aeronautics and Space Administration (NASA) has also proposed to use PPM in various free-space communication applications [5].

Examples of modulation techniques derived from PPM are multiple PPM (MPPM) [6], combinatorial PPM (CPPM) [7], and overlapping PPM (OPPM) [8]. Differential PPM (DPPM) is a simple modification of PPM that can achieve improved power and/or bandwidth efficiency. Hard-decision decoding of DPPM on photon-counting channels is analyzed with the window technique in [9]. It is shown that over such channels, DPPM achieves a higher cutoff rate than PPM for a certain range of physical parameters. In [10], it is shown that DPPM is superior to PPM in optical multiple-access applications. However, channels featuring additive white Gaussian noise (AWGN), such as the infrared wireless channel, are fundamentally different from the photon-counting channel, and the assumptions made in the window technique cause an underestimate of the performance of DPPM. In this paper, we evaluate the performance of optimal soft-decision decoding and hard-decision decoding of DPPM on AWGN channels.

Although infrared channels are not subject to multipath fading, they are subject to multipath dispersion, which causes intersymbol interference (ISI). The effects of ISI are especially severe in diffuse and high bit-rate systems. The ISI power penalties for on–off keying (OOK) and PPM are studied in [11] and [12]. Methods to combat ISI include optimal maximum-likelihood sequence detection (MLSD), equalization, and trellis coding [11]–[13]. We analyze the performance of DPPM over ISI channels and find that it incurs penalties similar to those of OOK and PPM.

The remainder of this paper is organized as follows. In Section II, we review the channel and noise models appropriate for wireless infrared communications. In Section III, the power requirements of hard-decision DPPM are analyzed on ideal and dispersive channels. In Section IV, we discuss the difficulties of implementing soft decisions and present approximate bounds on the error rate with MLSD. In Section V, we propose and analyze two equalization schemes for DPPM. The power spectral density (PSD) of uncoded DPPM signal is presented in Section VI. Methods to remove or mitigate the nonuniform bit-rate problem are proposed in Section VII. Concluding remarks can be found in Section VIII.

II. Channel and Noise Models

Coherent optical detection is not feasible in the indoor wireless infrared communication environment. Practical wireless infrared links use intensity modulation and direct detection (IM/DD). The appropriate channel model combines the intensity-modulation constraint of photon-counting channel with the multipath distortion and AWGN of conventional radio channels [1], [12]. An IM/DD system has an equivalent baseband model that hides its carrier frequency. Let $x(t)$

Paper approved by O. K. Tonguz, the Editor for Optical Transmission Systems of the IEEE Communications Society. Manuscript received September 15, 1997; revised September 15, 1998. This research was supported by the National Science Foundation Grant ECS-9710065, the Hewlett-Packard Company, and the University of California MICRO Program.

The authors are with the Department of Electrical Engineering and Computer Sciences, University of California, Berkeley, CA 94720 USA (e-mail: dsshiu@eecs.berkley.edu; jmk@eecs.berkley.edu).

Publisher Item Identifier S 0090-6778(99)06298-4.

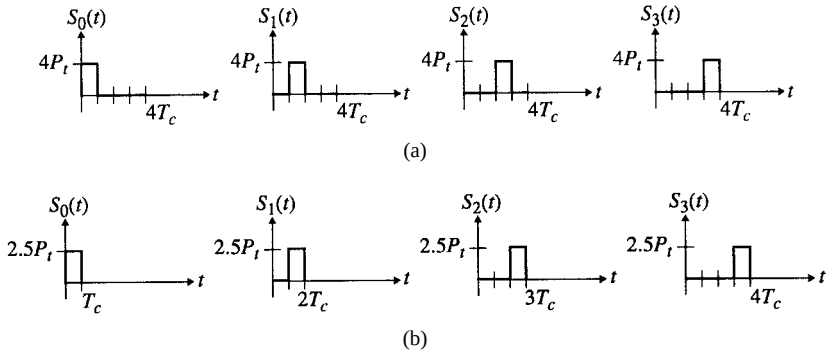

Fig. 1. Waveforms for (a) 4-PPM and (b) 4-DPPM using rectangular pulses. P_t represents the average transmitted power and T_c represents the chip duration.

represent the instantaneous optical power of the transmitter. The constraints on $x(t)$ are

$$x(t) \geq 0 \quad \text{and} \quad \lim_{T\to\infty} \frac{1}{2T} \int_{-T}^{T} x(t)\, dt \leq P_t \tag{1}$$

where P_t is the average optical-power constraint of the transmitter. The received photocurrent is

$$y(t) = Rh(t) \otimes x(t) + n(t) \tag{2}$$

where R is the photodetector responsivity and $h(t)$ is the channel impulse response, which is fixed for a given configuration of transmitter, receiver, and intervening reflectors. The received average optical power is $P = P_t H(0)$, where the channel dc gain is $H(0) = \int_{-\infty}^{\infty} h(t)\, dt$.

The optical IM/DD channel is often modeled by a signal-dependent Poisson-rate photon-counting model. Wireless infrared links are subject to intense ambient light that gives rise to a high-rate, signal-independent shot noise, which can be modeled as white and Gaussian [1], [12]. When such ambient light is absent, the dominant noise is preamplifier thermal noise, which is Gaussian. Thus, we model $n(t)$ as white, Gaussian, and independent of signal $x(t)$. Infrared links are also subject to cyclostationary noise arising from fluorescent lighting [14], which we neglect here.

ISI caused by multipath can be neglected at symbol rates below about 10 MBd in diffuse systems and about 100 MBd in directional, line-of-sight systems [16]. To assess the effect of ISI, some previous studies have employed an ensemble of measured channel responses [16]. We model multipath dispersion using the ceiling-bounce model developed by Carruthers and Kahn [17]. This model has been shown to quantify ISI effects with high accuracy. The channel impulse response is given by

$$h(t;\, a) = H(0) \frac{6a^6}{(t+a)^7}\, u(t) \tag{3}$$

where $u(t)$ is the unit step function. The parameter a depends on the room size and the transmitter and receiver positions and is related to the rms delay spread D by

$$D = \frac{a}{12}\sqrt{\frac{13}{11}}. \tag{4}$$

TABLE I
EXAMPLES OF MAPPINGS BETWEEN SOURCE BITS AND TRANSMITTED CHIPS FOR 4-PPM AND 4-DPPM

Source bits	Corresponding 4-PPM chips (nominal mapping)	Corresponding 4-DPPM chips (nominal mapping)	Corresponding 4-DPPM chips (reverse mapping)
00	1000	1	0001
01	0100	01	001
10	0010	001	01
11	0001	0001	1

III. HARD-DECISION DETECTION OF DPPM

A. PPM and DPPM

PPM is a well-known orthogonal modulation technique [18]. In L-PPM, a block of $\log_2 L$ input bits is mapped to one of L distinct waveforms, each including one "on" chip and $L-1$ "off" chips. A pulse $p(t)$ is transmitted during the "on" chip. DPPM is a simple modification of PPM. A DPPM symbol is obtained from the corresponding PPM symbol by deleting all of the "off" chips following the "on" chip. Specifically, the L-DPPM symbol set $s_n(t)$, $0 \leq n \leq L-1$, using rectangular pulses, is

$$s_n(t) = \begin{cases} 0 & t < nT_c \\ P_c & nT_c \leq t \leq (n+1)T_c \end{cases} \tag{5}$$

where P_c is the peak power and T_c is the chip duration. The signal waveforms of PPM and DPPM are shown in Fig. 1. PPM and DPPM can also be conceived as block codes over OOK links. The DPPM or PPM encoder first transforms the source bit sequence into a chip sequence according to the DPPM or PPM coding rule, such as the ones shown in Table I. Note that the code rate of DPPM is not constant. The chip sequence is subsequently transmitted by an OOK transmitter using a pulse shape $p(t)$. Fig. 2(a) shows the block diagram of a DPPM transmitter.

One of the advantages of DPPM over PPM is that symbol synchronization, which is an important requirement for PPM detection, is not necessary with DPPM. But more importantly, DPPM achieves higher power and bandwidth efficiency than PPM. Before presenting the error-rate analysis of DPPM, we will provide an intuitive explanation of its better average-

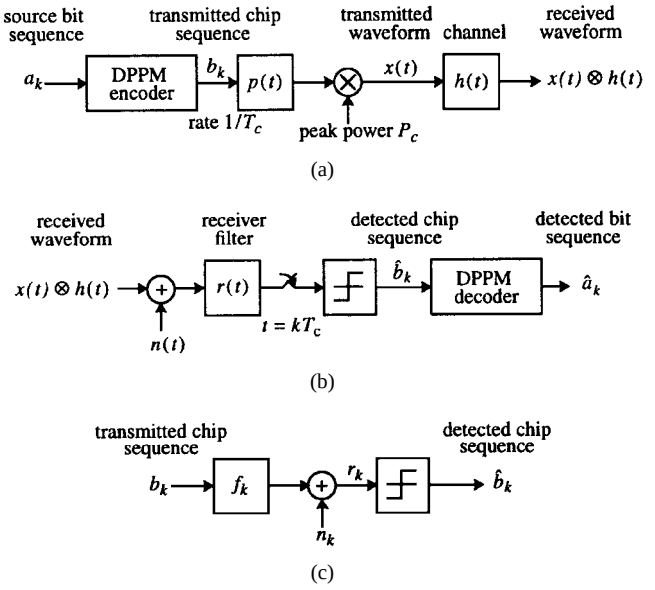

Fig. 2. (a) Configuration-time block diagram of the DPPM transmitter. The "on" chips in the transmitted sequence induce generation of a unit-amplitude pulse $p(t)$ of duration T_c. (b) Continuous-time block diagram of unequalized hard-decision DPPM receiver. The receiver filter $r(t) = p(-t)$ is matched to the transmitted pulse shape. (c) Discrete-time equivalent system for the communication of the chip sequence. The equivalent discrete-time impulse response is $f_k = P_c p(t) \otimes h(t) \otimes p(-t)|_{t=kT_c}$.

power efficiency. In L-PPM, as L is increased, the average-power efficiency improves while the bandwidth efficiency is reduced. This results from increased signal-set dimensionality and higher peak-to-average ratio. In DPPM, we omit the redundant "off" chips following the "on" chip without substantially affecting the error probability. For a fixed L, L-DPPM has a higher duty cycle and, thus, is *less* average-power efficient than L-PPM. However, for a fixed-average bit rate and fixed-available bandwidth, one can employ a higher L with DPPM than with PPM, resulting in a net improvement in average-power efficiency.

The fact that DPPM symbols do not have equal duration complicates the analysis and application of DPPM. Note that a single-chip error not only corrupts the bits directly associated with that chip, but also shifts the bits that follow those bits. This makes the usual definition of bit error rate (BER) a meaningless performance measure for DPPM. In our analysis, we compare modulation schemes in terms of packet-error rate because most data networks in use today employ error detection and automatic-retransmission requests for error control. Another distinct property resulting from the nonuniform symbol length is that the symbol boundaries are not known prior to detection. The optimal soft decoding of DPPM requires use of MLSD, even in the absence of error-control coding or ISI. Furthermore, the Viterbi algorithm is not applicable. Therefore, most practical implementations of DPPM would probably employ hard-decision decoding.

B. Error-Probability Analysis

Fig. 2(b) shows the continuous-time block diagram of a hard-decision detection DPPM receiver. The received signal is passed through a receiver filter $r(t) = p(-t)$ matched to the transmitter pulse; a slicer at the filter output determines whether chips are "on" or "off." Fig. 2(c) shows the equivalent discrete-time system for obtaining the detected chip sequence. The discrete-time impulse response is $f_k = P_c p(t) \otimes h(t) \otimes r(t)|_{t=kT}$, where $h(t)$ is the channel impulse response. Unless the channel is nondispersive, i.e., the rms delay spread is zero, f_k contains a zero tap, a single precursor tap, and possibly multiple postcursor taps.

We first consider a DPPM system transmitting over a nondispersive channel. Let p_0 denote the probability that an "off" chip is detected to be "on," and vice versa for p_1. Throughout this work, we will model the input bit stream to be an independently, identically distributed (i.i.d.) Bernoulli $(1/2)$ process. The packet-error rate for an F-bit, N-chip packet is

$$\begin{aligned} P_{F,\,\mathrm{DPPM}} &= 1 - (1-p_0)^{N-(F/\log_2 L)}(1-p_1)^{(F/\log_2 L)} \\ &\approx \left(N - \frac{F}{\log_2 L}\right) p_0 + \frac{F}{\log_2 L}\, p_1. \end{aligned} \tag{6}$$

If the threshold is set at the mean of expected "on" and "off" levels, e.g., $P_0 = P_1$, then

$$P_{F,\,\mathrm{DPPM}} \approx NQ\left(RP_t\sqrt{\frac{(L+1)\log_2 L}{8R_bN_0}}\right) \tag{7}$$

where N_0 is the (two-sided) noise PSD and $R_b = \log_2 L/(L+1)T_c$ is the average bit rate. Choosing $\theta = f_0/2$ is found to introduce less than 0.1-dB optical power penalty at practical packet lengths and packet-error rates, as compared to the optimally chosen threshold. As shown in Section VI, the bandwidth required to support communications at bit rate R_b is $W = (L+1)R_b/2\log_2 L$ using L-DPPM, $W = LR_b/\log_2 L$ using L-PPM, and $W = R_b$ using OOK [12].

Throughout this paper, we normalize all power requirements to the power required by OOK to send a 1-kB packet at average packet-error rate of 10^{-6}. The error probability for an F-chip OOK packet is $P_{F,\,\mathrm{OOK}} \approx NQ(RP_t/(R_bN_0)^{1/2})$ and for an F-chip PPM packet is $P_{F,\,\mathrm{PPM}} \approx NQ(RP_t(L\log_2 L/4R_bN_0)^{1/2})$ [12]. In Fig. 3, we display the average optical power and bandwidth requirements of OOK, PPM, and DPPM. Among many choices of L-DPPM, 16-DPPM is especially attractive. It provides a 3-dB optical average-power gain over 4-PPM, the modulation format adopted in the IrDA finite impulse response standard [4], and requires just slightly more bandwidth. 16-DPPM also supports the same bit rate as 16-PPM using less than half of the bandwidth, albeit at 1.4-dB higher average power.

We now consider using unequalized hard-decision detection of DPPM and PPM on dispersive channels. The slicer compares the receiver filter output r_k to a threshold θ to obtain $\hat{b}_k$, the estimate of chip b_k

$$\hat{b}_k = 1 \text{ iff } r_k \geq \theta. \tag{8}$$

The average chip-error probability is calculated as follows. Note that f_k contains a zero tap, a single precursor tap, and possibly multiple postcursor taps. Suppose that the duration of f_k is m taps. Let s be an m-chip segment randomly taken from a (very long) DPPM packet, $p(s)$ be the probability

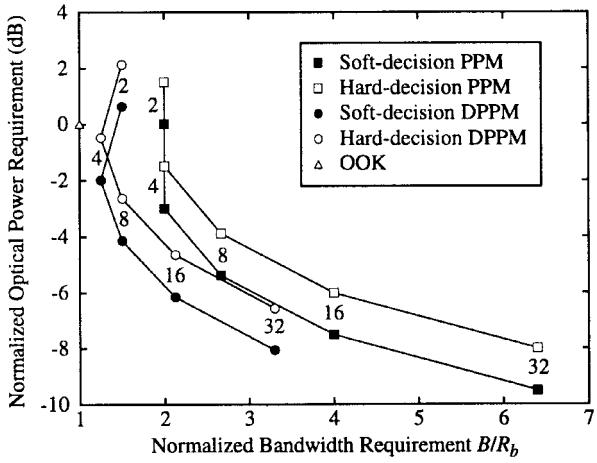

Fig. 3. Comparison of average-power efficiency and bandwidth efficiency of PPM, DPPM, and OOK on nondispersive channels. Both soft-decision and hard-decision detection are considered. The normalized power and bandwidth requirements of OOK are set to 0 dB and 1, respectively. The numbers represent values of L, the PPM, and DPPM orders.

of occurrence of s, and $I(s)$ be the receiver filter output (excluding noise) of the next-to-last chip of s. The error probability of the next-to-last chip of s is $\varepsilon(s) = Q((\theta - I(s))/(N_0)^{1/2})$ if it is an "off" chip or $Q((I(s)-\theta)/(N_0)^{1/2})$ if it is an "on" chip. The average chip-error rate for DPPM or PPM is

$$P_c = \sum_s p(s)\varepsilon(s) \tag{9}$$

summed over all possible s.

The error rates in the above analysis are functions of the slicer threshold. Because "off" chips are more likely than "on" chips, the optimum threshold θ^*, which minimizes the chip-error rate, cannot be chosen as $f_0/2$, as on nondispersive channels. The optimum threshold θ^* is a complicated function of the signal and noise powers, the impulse response f_k, and the order L, and is determined here by numerical optimization. On dispersive channels, for a fixed channel dc gain, the optimum threshold θ^* is found to decrease as the delay spread increases.

In addition to the optimum threshold, we consider two heuristic thresholds. Heuristic threshold "type 1" is defined by $\theta_1 = \frac{1}{2}\sum_k f_k$, and "type 2" is defined by $\theta_2 = \frac{1}{2}E(r_k|b_{k=1}) + \frac{1}{2}E(r_k|b_{k=0})$. The optical power requirements for unequalized DPPM and PPM systems, using optimum type 1 and type 2 thresholds, are displayed in Fig. 4. The type 1 heuristic threshold performs nearly as well as the optimum threshold. The type 2 heuristic threshold leads to a significant performance degradation and also leads to error-rate floors at much lower delay spreads than the other two threshold choices. The type 1 heuristic threshold can be implemented in practice by observing the total power received when isolated "on" chips are transmitted.

If the x- and y-axes in Fig. 4 are changed to represent the ratio of delay spread to chip duration and the optical power penalty due to ISI, respectively, it can be seen that the relationship between these two quantities is very nearly the same for all values of the DPPM order L. The same

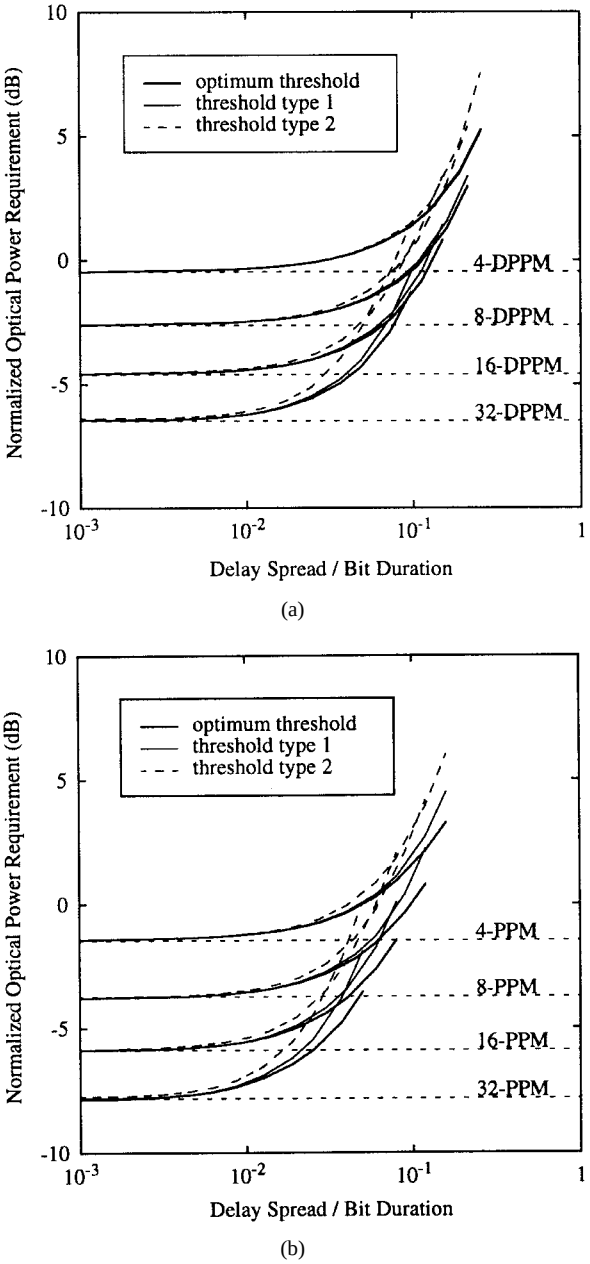

Fig. 4. Average optical-power requirements to transmit a (a) 1-kB DPPM packet and (b) 1-kB PPM packet at 10^{-6} packet-error rate using unequalized hard-decision detection with various threshold choices. The reference level (0 dB) is the optical power required for OOK on a nondispersive channel.

phenomenon has also been observed for PPM [11]. At a given ratio of rms delay spread to chip duration, the ISI penalty is slightly larger for DPPM than for PPM.

IV. Maximum-Likelihood Sequence Detection of DPPM

A. MLSD on Nondispersive Channels

Because the symbol boundaries are not known prior to detection, the optimal soft decoding of DPPM requires use of MLSD, even in the absence of ISI or error-control coding. In other words, to detect an N-chip DPPM packet which encodes F bits, the likelihoods of all possible F-bit packets with the same packet length must be compared.

Considering each received chip sample to represent an orthogonal dimension, the ML detection criterion is seen to correspond to minimum-Euclidean-distance detection. The minimum-distance errors correspond to situations when the detected packet and the transmitted packet differ in the position of one particular "on" chip. The Hamming distance between these two packets is two. With DPPM, in contrast to PPM, a minimum-distance error packet can be constructed by removing an "on" chip and placing it anywhere in the packet, as long as the resulting packet does not have a run of more than L "off" chips. The number of packets lying at Hamming distance two from a given packet is not constant. An estimate for this number is $((L-1)/4)(F/\log_2 L)^2$; this estimate employs the fact that the average packet length measured in chips is $\overline{N} = (F/\log_2 L)((L+1)/2)$ and approximately half of the "on" chips correspond to the aforementioned case. For short packets, simulation shows that this is a good approximation. At high signal-to-noise ratio (SNR), minimum-distance errors dominate. An approximate upper bound of the packet-error probability at high SNR is thus

$$P_{F,\,\mathrm{DPPM}} \cong \left(\frac{L-1}{4}\right)\left(\frac{F}{\log_2 L}\right)^2 \cdot Q\left(RP_t\sqrt{\frac{(L+1)\log_2 L}{4R_bN_0}}\right). \quad (10)$$

B. MLSD on Dispersive Channels

The equivalent discrete-time model [11], [18] used to study MLSD and equalization techniques on ISI AWGN channels is shown in Fig. 5. The continuous-time system consists of the transmitter filter $p(t)$, the channel impulse response $h(t)$, a matched filter $r(t) = p(-t) \otimes h(-t)$, a whitening filter $W(z)$, which is the inverse of the maximum-phase part of $h_k = p(t) \otimes h(t) \otimes r(t)|_{t=kT_c}$, and a detection device. The discrete-time channel impulse response is $g_k = P_c h_k \otimes w_k$. Nonnegativity is enforced on $p(t)$, $h(t)$, $r(t)$, and g_k because they represent optical power. We note that the g_k are proportional to the transmitted optical power.

To calculate the packet-error probability using MLSD, we follow a procedure similar to that introduced by Forney [19]. Let $\overline{e}$ be a vector over $\{-1, 0, 1\}$; the leading and ending entries of $\overline{e}$ are nonzero. We define $\overline{e}$ to be an *error unit* if it does not contain any run of zeros longer than the number of postcursor taps of f_k. An MLSD-detected packet can contain any number of nonoverlapping error units, as long as the overall chipwise sum of these error units is zero, to conserve the number of symbols. In *singlet* error events, the detected packet contains a single error unit. In doublet error events, it contains two error units, and the chipwise sum of either error unit is nonzero. (Note that a doublet error event is not equivalent to a combination of two singlet error events.) If the length of the packet is not very long (i.e., less than 1 kB), we find that at high SNR, singlet and doublet error events dominate the packet errors. Let S be the set containing all error units $\overline{e}$ causing singlet errors and D be the set of all error unit pairs $(\overline{e}^1, \overline{e}^2)$ causing doublet errors. The packet-error rate

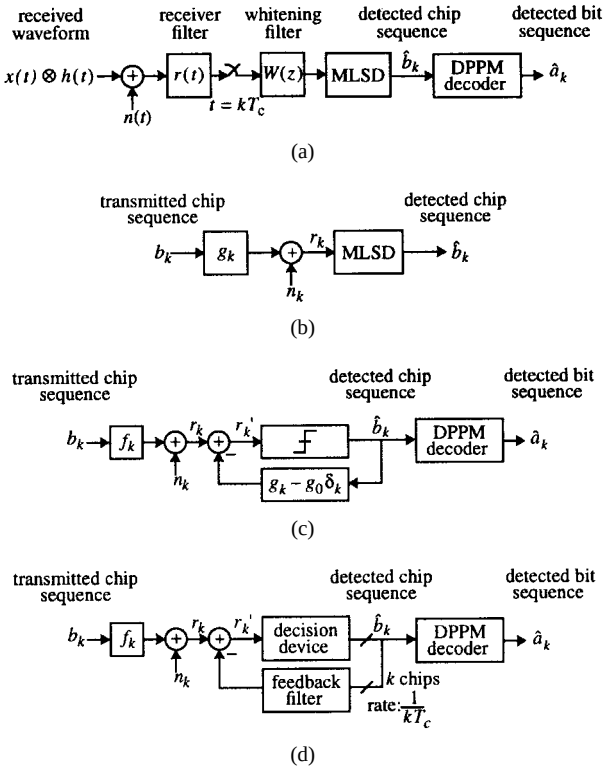

Fig. 5. (a) Continuous-time block diagram of whitened-matched-filtered MLSD receiver. The matched filer is $r(t) = p(-t) \otimes h(-t)$ and the maximum-phase whitening filter $W(z)$ is specified by $W(z)W(-z) = Z\{P_c p(t) \otimes h(t) \otimes r(t)|_{t=KT_c}\}$. (b) Discrete-time equivalent system for obtaining the detected chip sequence. The discrete-time equivalent impulse response is $g_k = [P_c p(t) \otimes h(t) \otimes r(t)|_{t=KT_c}] \otimes W_k$. (c) Block diagram for hard-decision chip-rate DFE. (d) Block diagram for multichip-rate DFE.

can be approximately upper bounded by

$$P_{F,\,\mathrm{DPPM}} \approx \sum_{\overline{e}\in S} \alpha(\overline{e}) Q\left(\frac{1}{2}\sqrt{\frac{\sum_k |e_k \otimes g_k|^2}{N_0}}\right) + \left(\sum_{(\overline{e}^1,\overline{e}^2)\in D} \frac{F}{2}\,\alpha\big(e_k^1, e_k^2\big) \cdot Q\left(\frac{1}{2}\sqrt{\frac{\sum_k |e_k^1 \otimes g_k|^2 + \sum_k |e_k^2 \otimes g_k|^2}{N_0}}\right)\right) \quad (11)$$

where $\alpha(\overline{e})$ and $\alpha(\overline{e}^1, \overline{e}^2)$ are the prior probabilities for $\overline{e}$ and $(\overline{e}^1, \overline{e}^2)$. The upper bounds of packet-error probability for OOK and PPM can be similarly found to be

$$P_{F,\,\mathrm{OOK}} \le \sum_{\overline{e}} 2^{-H(\overline{e})} Q\left(\frac{1}{2}\sqrt{\frac{\sum_k |e_k \otimes g_k|^2}{N_0}}\right) \quad (12)$$

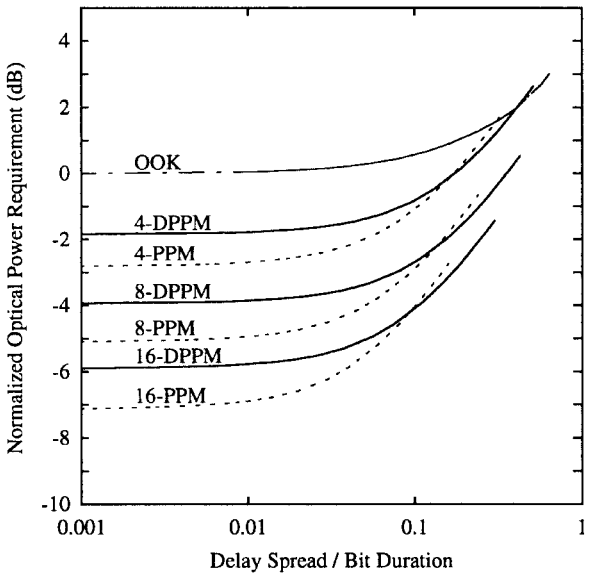

Fig. 6. Optical-power requirement to transmit a 1-kB packet at 10^{-6} packet-error with MLSD.

and

$$P_{F,\mathrm{PPM}} \le \sum_{\overline{e}} L^{-H(\overline{e})} Q\left(\frac{1}{2}\sqrt{\frac{\sum_k |e_k \otimes g_k|^2}{N_0}}\right) \quad (13)$$

where $H(\overline{e})$ is the number of nonzero entries in the error event $\{\overline{e}\}$. The average optical power requirements of OOK, PPM, and DPPM with MLSD are shown in Fig. 6.

We would like to point out that the dispersive IM/DD channel conserves the transmitter power but spreads it out in time. The Euclidean distance between "off" and "on" chips is reduced, since $(\sum g_k^2 \le \sum g_k)^{1/2}$. This means that once a pulse is spread out, the "effectiveness" of the optical power is reduced and cannot be recovered.

V. DPPM WITH DECISION-FEEDBACK EQUALIZATION

Decision-feedback equalizers (DFE's) are used in many applications to mitigate ISI. Zero-forcing (ZF) decision-feedback chip-rate and symbol-rate equalization for PPM are proposed and analyzed, respectively, by Barry [12] and Audeh *et al.* [20]. Although the minimum-mean square-error (MMSE) DFE generally offers better performance than ZF-DFE, we only consider ZF-DFE DPPM systems in our analysis because at low-error rates, the two types of equalizers exhibit nearly identical performance and because the ZF-DFE is easier to analyze. In the following, we use the equivalent discrete-time whitened matched-filtered front-end shown in Fig. 5.

A. Chip-Rate DFE

The diagram of a hard-decision chip-rate DFE system is shown in Fig. 5(c). Assuming that the slicer threshold is $g_0/2$ in the absence of error propagation, the chip-error probability is

$$P_c = Q\left(\frac{g_0}{2\sqrt{N_0}}\right). \quad (14)$$

When compared to the ISI-free channel, the optical power penalty is $-10\log(g_0/P_c)$ dB. By employing the appropriate technique to reconstruct symbol sequence from the detected chip sequence, this chip-rate DFE can be applied with DPPM, PPM, and OOK.

B. Multichip-Rate DFE

The chip-rate equalizer makes hard decisions on a chip-by-chip basis, utilizing only the transmitted energy in the zero tap of the WMF impulse response in making the decision. One would expect to obtain better performance by using a trellis detector in place of the memoryless threshold device. In this section, we investigate the gain that can be achieved by using a more sophisticated decision device.

In Fig. 5(d), suppose that the decision device has access to the n most recent received chip samples $\{r_i'\}_0^{n-1}$. The postcursor ISI from $\{b_i\}$, $i<0$, in $\{r_i'\}_0^{n-1}$ is completely removed by ZF-DFE. The decision device forms a local maximum-likelihood decision of the k transmitted chips $\{b_i\}_0^{k-1}$ based on $\{r_i'\}_0^{n-1}$. That is, it chooses a binary sequence $\{\hat{b}_i\}_0^{n-1}$ to minimize the quantity $\sum_{i=0}^{n-1}(r_i' - \hat{b}_i \otimes g_i)^2$, and the first k chips of $\{\hat{b}_i\}_0^{n-1}$ are declared as the decisions for $\{b_i\}_0^{k-1}$. These decisions are used to remove the ISI, and the process is repeated for $\{b_i\}_k^{2k-1}$. In contrast to the chip-rate DFE, the detection and feedback take place every k chips. Therefore, the structure shown in Fig. 5(b) is henceforth called the multichip-rate equalizer. The multichip-rate DFE can also be used with DPPM, PPM, and OOK.

In the absence of error propagation, the decision-error probability conditioned on the n most recently transmitted chips $\{b_i\}_0^{n-1}$ can be upper-bounded by

$$P(b^n) \le \sum_{c^n} Q\left(\frac{d(b^n, c^n)}{2\sqrt{N_0}}\right). \quad (15)$$

Here, we write b^n for $\{b_i\}_0^{n-1}$, and $d(b^n, c^n) = (\sum_{k=0}^{n-1}\{(b_k - c_k)\otimes g_k\}^2)^{1/2}$ is the Euclidean distance between the first n samples of $b^n \otimes g_k$ and those of $c^n \otimes g_k$. The summation is taken over all n-chip sequences c^n whose first k chips are not identical to the first k chips of b^n. Let the prior probability of b^n be $w(b^n)$, which depends on the modulation format. The average decision-error probability is

$$P = \sum_{b^n} w(b^n) P(b^n). \quad (16)$$

The error probability of the multichip-rate DFE with OOK can be calculated using $w(b^n) = 2^{-n}$. With PPM and DPPM, in order to simplify the error-rate calculation, we will consider the transmitted chip distribution to be OOK-like. That is, we take $w(b^n) = 2^{-n}$ for PPM and DPPM, regardless of the order L. This is a plausible simplification because the actual chip distribution is much less important than the chip SNR (see Section III). The average optical power requirements for 4-

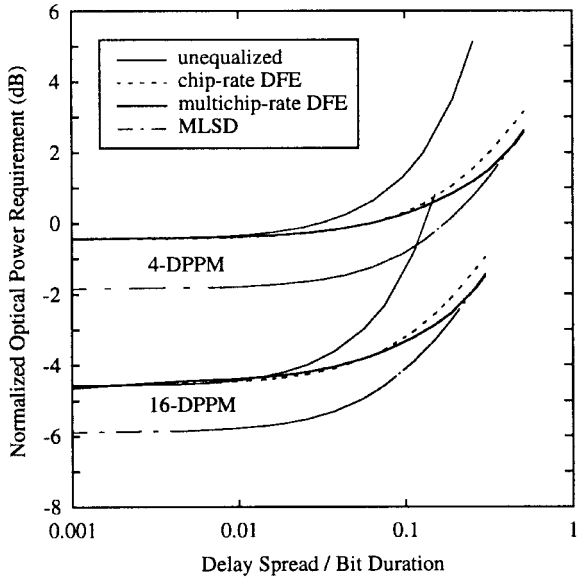

Fig. 7. Average optical-power requirement to transmit a 1-kB packet with 10^{-6} packet-error rates using 4- and 16-DPPM. The unequalized system employs hard decisions with an optimum threshold. The power requirements for unequalized and chip-rate DFE and MLSD systems represent upper bounds.

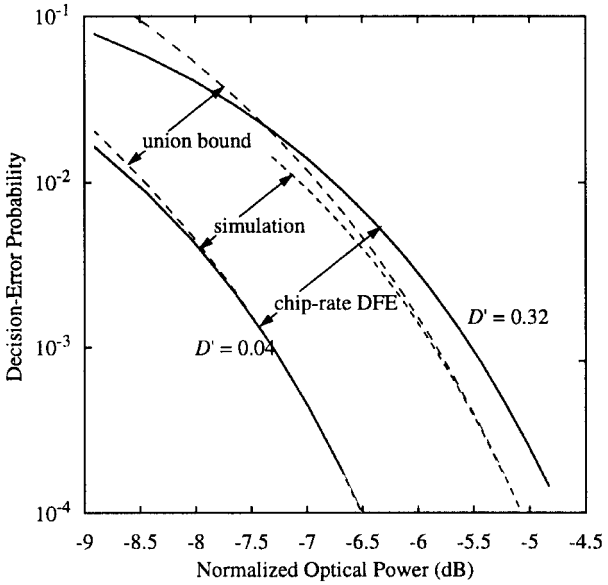

Fig. 8. Decision-error probability for multichip-rate DFE as a function of normalized optical power for 16-DPPM. D' represents the ratio of rms delay spread to chip duration. The equalizer parameters used are $(n, k) = (2, 1)$ at $D' = 0.04$ and $(n, k) = (4, 1)$ at $D' = 0.032$. At low decision-error rates, the union bound (16) merges with the simulation results. At decision-error rates higher than 10^{-3}, the union bound is loose, and the performance of the chip-rate DFE serves as a tighter upper bound. The reference optical power (0 dB) is set at the power required to transmit a 1-kB packet with 10^{-6} BER using OOK.

and 16-DPPM with both chip-rate and multichip-rate equalizers are shown in Fig. 7. The parameters for the multichip-rate DFE are $(n, k) = (4, 1)$. As expected, both equalizers extend the useful operating range to higher delay spreads. For a 3-dB average optical power penalty, the chip-rate equalized system can tolerate a delay spread approximately three times higher than the unequalized system. The multichip-rate equalized system yields a 0.5-dB optical power gain over the chip-rate equalized system at this delay spread level. Fig. 8 shows the decision-error probability versus optical power for 16-DPPM with multichip-rate DFE.

In the Monte Carlo simulation, an i.i.d. Bernoulli (1/2) sequence is fed into the DPPM transmitter of Fig. 5(a) to generate the transmitted chip sequence. Simulation allows us to observe the error-propagation effects inherent in DFE. In Fig. 8, the error-probability curve from Monte Carlo simulation merges with the upper bound (16) at chip-error rates below approximately 10^{-4}. This demonstrates the tightness of the upper bound and also justifies our simplifying assumptions.

The channel rms delay spread affects the optimum choice of the parameters (n, k). First, we find that given a fixed $n-k$, the decision-error probabilities for DFE's with different k are close to each other. Increasing k reduces the number of decisions per packet. As a result, the packet-error rate is lowered. However, larger k introduces higher complexity because the number of Euclidean distance calculations per detected chip is proportional to $2^k/k$. Second, we have found that the difference between n and k need not be large, even at high delay spreads. By simulation, we have found that when the rms delay spread is 64% of the chip duration T_c, the equalizer gain with $(n, k = 1)$ saturates after $n \geq 4$.

We should point out that this multichip-rate DFE is fundamentally different from the symbol-rate DFE for PPM introduced in [20]. The latter inherently uses symbol-by-symbol soft decisions. The multichip-rate DFE neglects the underlying symbol structure; therefore, it can never achieve performance approaching MLSD.

VI. Spectral Properties of DPPM

As shown in Fig. 2(a), the transmitted DPPM waveform is $x(t) = \sum_{k=-\infty}^{\infty} b_k p(t - kT_c)$. We can view $x(t)$ as a cyclostationary process and compute its PSD by using $S_x(\omega) = (1/T_c)S_b(\omega)|P(\omega)|^2$. For a rectangular pulse $p(t)$, $|P(\omega)|^2 = T_c^2 \operatorname{sinc}^2(\omega T_c/2\pi)$, where we use the definition $\operatorname{sinc}(x) \equiv \sin(\pi x)/\pi x$. $S_b(\omega)$, the PSD of the chip sequence, is given by the discrete-time Fourier transform of the chip autocorrelation function r_k, which is defined by $r_{n-m} \equiv E(b_n b_m)$. The recurrence relationship for r_k is

$$r_k = \frac{2}{L+1} \sum_{j=1}^{\min\{L,k-1\}} \Pr(b_k = 1, b_{k-1} = \cdots = b_{k-j+1} = 0, b_{k-j} = 1 | b_0 = 1) \tag{17}$$

which can be simplified to $r_0 = 2/(L+1)$ and

$$r_k = \begin{cases} \dfrac{2}{L^k}(L+1)^{k-2} & 1 \leq k \leq L \\ \dfrac{1}{L}\displaystyle\sum_{i=1}^{L} r_{k-i} & k > L. \end{cases} \tag{18}$$

The solution for r_k, $k > L$ is given by $r_k = \sum_{i=1}^{L} c_i x_i^k$. The x_i are the roots of the equation $x^L = (1/L)(x^{L-1} + x^{L-2} + \cdots + 1)$. The constraints of r_k, $k = 0, 1, \ldots, L-1$ determine c_i. It is not difficult to show that one of the x_i has value

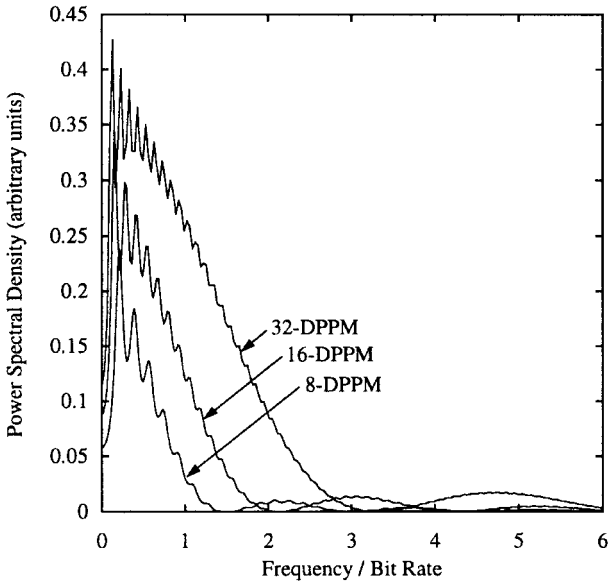

Fig. 9. PSD of 8-, 16-, and 32-DPPM. The transmitter pulse shape is rectangular. The various curves are normalized so that they represent the same average transmitted optical power.

one, and that all other x_i have absolute values strictly less than one. Therefore, r_k converges to a constant $(2/(L+1))^2$ asymptotically, in accordance to the intuition that two chips far away from each other have little correlation between them.

We find that $S_b(\omega) = S_c(\omega) + S_d(\omega)$, where $S_c(\omega)$ is a continuous component, and $S_d(\omega)$ is a discrete component that arises from the nonzero mean of the chip sequence. We find that

$$S_c(\omega) \cong \sum_{k=-5L}^{5L} \left[r_k - \left(\frac{2}{L+1} \right)^2 \right] \exp(-jk\omega) \quad (19)$$

and

$$S_d(\omega) = \frac{2\pi}{T_c} \left(\frac{2}{L+1} \right)^2 \sum_{k=-\infty}^{\infty} \delta\left(\omega - \frac{2\pi k}{T_c} \right). \quad (20)$$

We present the spectra for 8-, 16-, and 32-DPPM in Fig. 9, omitting the discrete spectral lines. The bandwidth occupied by the first spectral lobe of either DPPM or PPM signals is equal to the inverse of the chip duration. It can be seen that the continuous part of the PSD of DPPM does not approach zero at low frequencies, in contrast to PPM. If highpass filtering is employed to reduce the effect of fluorescent light noise or if the channel has a highpass nature, DPPM signals are subject to greater distortion than PPM signals for a fixed highpass filter cutoff frequency.

VII. System Design Issues

An unusual characteristic of DPPM is that the time required to transmit a packet containing a fixed number of bits is not constant because the DPPM symbols do not have equal durations. The average bit rate is $\overline{R}_b = 2/(L+1)T_c$. The actual bit rate, however, varies from $((L+1)/2L)\overline{R}_b$ to $((L+1)/2)\overline{R}_b$. Packets that require excessive time to transmit can cause transmitter buffer overflow or unacceptable delay of real-time applications, and provisioning for such packets can lead to inefficient utilization of network resources. Packets requiring too little transmission time can cause transmitter buffer underflow, receiver buffer overflow, or a temporary violation of eye-safety requirements.

In the following, we propose two techniques to reduce bit-rate variations. They place different demands upon the network: the first method requires the transmitter to examine the packet contents prior to transmission, and the second requires the use of large packets and relies upon special procedures to transmit packets that would otherwise require excessive transmission time. Both techniques introduce minimal complexity and overhead.

A. Networks Requiring Fixed Throughput

In some networks, every packet containing a given number of source bits must require the same time for transmission. This can be achieved by exploiting the fact that the mapping between source bits and DPPM symbols can be chosen arbitrarily. Examples of two DPPM mapping rules, which we refer to as the "nominal" and the "reverse" mapping rules, are shown in Table I. The two mappings differ in that the roles of the m-chip symbol and the $(L-m+1)$-chip symbol are interchanged. If an input packet produces an F_1-chip DPPM packet under the nominal mapping rule, then under the reverse mapping rule it produces an F_2-chip packet, where the mean packet length is $(F_1+F_2)/2$. Thus, we can have the transmitter examine the packet, choose the mapping rule that yields a shorter packet length, add a flag chip indicating the choice of mapping rule at the beginning of transmission, and append "off" chips at the end of the packet until the packet duration reaches the mean packet duration. The packet duration and the per packet average power both meet exact requirements. Note that the reverse mapping can be easily implemented by applying the nominal mapping rule on the complemented input packets.

The main drawback of this technique is that the transmitter must determine the duration of the packet prior to encoding it, possibly resulting in processing delay. To reduce delay, a packet can be partitioned into M smaller blocks. The above algorithm is then applied in a block-by-block fashion, except that the additional "off" chips are appended after the last symbol of the packet to aid the receiver in maintaining proper synchronization. The latency is decreased by a factor of M; however, the overhead associated with the flag chips is increased by a factor of M.

B. Networks Not Requiring Fixed Throughput

Assuming that the input bit sequence is i.i.d. and uniform on {0, 1}, the probability that the packet duration deviates from the expected packet length by a factor of ε can be calculated approximately by using the central limit theorem. Such an approximation is found to be very accurate if the number of symbols in a packet exceeds 100. For example, to transmit a 2-kB 16-DPPM packet, the probability that the packet length is longer than the mean packet length by 10% is about 10^{-32}, which is essentially zero.

In some networks, packet transmission times are not required to be fixed. In such networks, it suffices to use a long scrambler and a large packet size to keep the probability of packets with excessively short or long duration under a desired value. Special procedures can be provided to process packets of abnormal duration, depending on the constraints of the network. These special procedures include rescrambling by another scrambling sequence, and partitioning the source packet into smaller units and retransmitting each one as an individual packet.

Variable packet transmission time has important implications for networks employing media-access control (MAC) protocols based on channel reservations. For example, the IrMAC [21], a MAC protocol being considered by the IrDA, attempts to minimize packet collisions through broadcasting channel reservation/release messages from both the transmitter and the receiver. In order to prevent the "hidden station" problem, whereby stations that fail to detect an ongoing communication start to transmit before the channel is idle, a station wishing to transmit needs to wait for a time interval equal to the mean packet duration plus a guard time before transmitting, unless it receives a channel release message. We note that as the packet duration becomes longer, there is a decrease in the ratio of the required guard time to the mean packet duration. If we model the packet length as a Gaussian random variable, the relation between the guard time GT and the probability ε that the duration of an F-bit packet is longer than the expected packet duration plus GT is

$$\varepsilon = Q\left(\frac{GT\sqrt{F/\log_2 L}}{\sigma T_c}\right) \tag{21}$$

where

$$\sigma^2 = \frac{1}{L}\sum_{k=1}^{L} k^2 - \left(\frac{L+1}{2}\right)^2 = \frac{L^2-1}{12}.$$

To cite another implication of variable packet duration: in order to minimize the power consumption of a portable transceiver, it is best to power down the transceiver until the channel is possibly free. Equation (21) can also be used to estimate the proper duration for transceivers to remain in the "sleep" mode.

VIII. Conclusion

We have assessed the performance of DPPM over infrared wireless channels. We have considered several receiver structures, including a simple, unequalized hard-decision receiver, an MLSD, a chip-rate DFE, and a multichip-rate DFE. We find that DPPM always achieves higher power efficiency and lower hardware complexity than PPM. These make DPPM a favorable candidate to replace PPM in many applications.

Using a simple model for the indoor wireless infrared channel, we find that the ISI penalties of DPPM are essentially determined by the ratio of the rms delay spread to chip duration. DFE is an effective technique to combat ISI. In addition to the conventional chip-rate DFE, we propose and analyze (n, k) multichip-rate equalization. We find that it offers better performance than the chip-rate DFE, particularly when the ISI is significant.

We derive the PSD of DPPM signals assuming that the transmit pulse shape is rectangular. The PSD does not approach zero at dc. Thus, if highpass filtering is employed to reduce the effect of fluorescent light noise, DPPM signals are subject to greater distortion than PPM signals.

We discuss the potential problems arising from the variable bit rate nature of DPPM. We propose two techniques to control the bit rate variation, which are appropriate for different network requirements.

Acknowledgment

The authors would like to thank S. Williams of Hewlett-Packard Laboratories for helpful discussions.

References

[1] J. M. Kahn and J. R. Barry, "Wireless infrared communications," *Proc. IEEE*, vol. 85, pp. 265–298, Feb. 1997.
[2] "Safety of laser products," International Electrotechnical Commission, CEI/IEC825-1, 1993.
[3] "Serial infrared (SIR) physical layer link specification," Infrared Data Association, Apr. 1994.
[4] "Fast serial infrared (FIR) physical layer link specification," Infrared Data Association, Jan. 1994.
[5] M. Fitzmaurice and R. Bruno, "NASA/GSFC program in direct detection optical communications for intersatellite links," in *Proc. Optical Space Communications Meeting*, Paris, France, Apr. 26–29, 1989, pp. 10–23.
[6] D. A. Fares, "Heterodyne detection of multipulse signaling in optical communication channels," *Microwave Opt. Technol. Lett.*, vol. 9, no. 4, July 1995.
[7] J. M. Budinger, M. Vanderaar, P. Wagner, and S. Bibyk, "Combinatorial pulse position modulation for power-efficient free-space laser communications," in *Proc. SPIE*, Los Angeles, CA, Jan. 20–21, 1993, pp. 214–225.
[8] T. Ohtsuki, I. Sasase, and S. Mori, "Lower bounds on capacity and cutoff rate of differential overlapping pulse position modulation in optical direct-detection channel," *IEICE Trans. Commun.*, vol. E77-B, pp. 1230–1237, Oct. 1994.
[9] D. Zwillinger, "Differential PPM has a higher throughput than PPM for the band-limited and average-power-limited optical channel," *IEEE Trans. Inform. Theory*, vol. 34, pp. 1269–1273, Sept. 1988.
[10] V. W. S. Chan, "A multiple-user random-access optical communication system," in *Proc. ICC'79*, pp. 01.4.1–01.4.5.
[11] M. D. Audeh, J. M. Kahn, and J. R. Barry, "Performance of pulse-position modulation on measured nondirected indoor infrared channels," *IEEE Trans. Commun.*, vol. 44, pp. 654–659, June 1996.
[12] J. R. Barry, *Wireless Infrared Communications.* Norwell, MA: Kluwer, 1994.
[13] D. C. Lee, J. M. Kahn, and M. D. Audeh, "Trellis-coded pulse-position modulation for indoor wireless infrared communications," *IEEE Trans. Commun.*, to be published.
[14] R. Narasimhan, M. D. Audeh, and J. M. Kahn, "Effect of electronic-ballast fluorescent lighting on wireless infrared links," in *Proc. IEE Optoelectronics*, Dec. 1996, vol. 143, no. 6, pp. 347–354.
[15] G. W. Marsh and J. M. Kahn, "Performance evaluation of experimental 50-Mb/s diffuse infrared wireless link using on–off keying with decision feedback equalization," *IEEE Trans. Commun.*, vol. 44, pp. 1496–1504, Nov. 1996.
[16] J. M. Kahn, W. J. Krause, and J. B. Carruthers, "Experimental characterization of nondirected indoor infrared channels," *IEEE Trans. Commun.*, vol. 43, pp. 1613–1623, Feb./Mar./Apr. 1995.
[17] J. B. Carruthers and J. M. Kahn, "Modeling of nondirected wireless infrared channels," *IEEE Trans. Commun.*, vol. 45, pp.1260–1268, Oct. 1997.
[18] J. G. Proakis, *Digital Communications*, 3rd ed. New York: McGraw-Hill, 1995.

[19] G. D. Forney, "Maximum-likelihood sequence estimation of digital sequences in the presence of intersymbol interference," *IEEE Trans. Inform. Theory*, vol. IT-18, pp. 363–378, May 1972.
[20] M. D. Audeh, J. M. Kahn, and J. R. Barry, "Decision-feedback equalization of pulse-position modulation on measured non-directed indoor infrared channels," *IEEE Trans. Commun.*, vol. 47, pp. 500–503, Apr. 1999.
[21] "Request for comments of advanced infrared IrMAC draft protocol specification," Infrared Data Association, Apr. 1997.

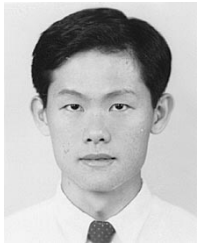

Da-shan Shiu (S'95) received the B.S.E.E. degree from the National Taiwan University in 1993. He is currently working toward the Ph.D. degree in the Department of Electrical Engineering and Computer Sciences at the University of California at Berkeley.

His current research interests include wireless optical communications, space-time signal processing, smart antenna, and W-CDMA.

Mr. Shiu is a member of the Phi Tau Phi.

Joseph M. Kahn (M'87–SM'98), for photograph and biography, see p. 260 of the February 1999 issue of this TRANSACTIONS.